13TH CANADIAN MASONRY SYMPOSIUM
HALIFAX, CANADA
JUNE 4TH – JUNE 7TH 2017

EXPERIMENTS TO DETERMINE THE OUT-OF-PLANE BEHAVIOUR OF CFRP AND DUCTILE ADHESIVE REINFORCED CLAY BRICK MASONRY WALLS

Türkmen, Ö.S.[1]; Vermeltfoort, A.T.[2]; Wijte, S.N.M.[3] and Martens, D.R.W.[4]

ABSTRACT

The reinforcement systems with ductile adhesive have shown to remarkably increase the out-of-plane flexural capacity of unreinforced masonry (URM). Extensive laboratory scale out-of-plane (OOP) experiments have been conducted with construction material that is representative for the masonry found in Groningen. The research purpose was to gain more understanding on the out of plane behaviour of carbon fibre reinforced polymer (CFRP) and ductile adhesive reinforced masonry. In the experimental testing program three different reinforcement configurations have been involved. The first configuration consisted of a CFRP strip placed in the heart of the masonry wallettes with a visco-elastic epoxy. The second configuration had an additional surface treatment based on a polymer. The third configuration was similar to the second one, however with a cement based surface treatment with imbedded CFRP net. The results of the experimental tests confirmed the strong increase in both the moment- and flexural capacity and supported the previously stated significant gain in ductility.

KEYWORDS: *masonry, CFRP, reinforcement, seismic, experiments*

INTRODUCTION

In Groningen, an area in the North-East of the Netherlands, earthquakes occur as a result of the subsidence of the ground at relatively shallow depth beneath the earth's surface. This is caused by the extraction of gas from the Groningen gasfield. These so-called "induced" earthquakes distinguish themselves from the common and well known "tectonic" earthquakes, which occur as a result of ground movements in the deep crust. Another distinctive aspect is that the soft claylike soil in Groningen transmits the vibrations better compared to a rocky soil. Research and

[1] PhD Candidate, Department of the Built Environment, Section Structural Design, Eindhoven University of Technology, P,O, Box 513, 5600 MB, Eindhoven, O.S.Turkmen@tue.nl
[2] Associate Professor, Department of the Built Environment, Section Structural Design, Eindhoven University of Technology, P,O, Box 513, 5600 MB, Eindhoven, A.T.Vermeltfoort@bwk.tue.nl
[3] Full Professor, Department of the Built Environment, Section Structural Design, Eindhoven University of Technology, P,O, Box 513, 5600 MB, Eindhoven, S.N.M.Wijte@tue.nl
[4] Full Professor, Department of the Built Environment, Section Structural Design, Eindhoven University of Technology, P,O, Box 513, 5600 MB, Eindhoven, D.R.W.Martens@tue.nl

measurements done by KNMI provides a contour plot of peak ground acceleration in Groningen [1]. The maximum value in this contour plot is 0.36g with a return period of 475 years.

The majority of buildings in Groningen is composed of unreinforced single leaf masonry designed for relatively moderate wind loads. Therefore it is essential to improve the earthquake resistance of the current buildings in the area to prevent building collapse, with likely casualties. Due to the slenderness of the load bearing walls, the lateral load bearing capacity is mostly critical.

Some key aspects need to be taken into account when selecting a suitable solution. Ductility is one of the most important requirements for all kinds of seismic resistance structures. Unreinforced masonry, which lacks ductility, often fails in a brittle manner. When it's shaken severely it cracks and falls apart in a number of pieces. Therefore it is essential to "tie it together". Prior research concluded that the existing materials used in stand-alone retrofit systems were insufficient and needed improvement [2]. By applying a special developed epoxy and combining two stand-alone seismic retrofit measures, an amplifying effect in terms of load bearing capacity and ductility was reached. The proposed patented seismic retrofit system, QuakeShield, was tested in bending on wallettes. Due to the rather small scale of the initial research, one of the conclusions pointed out the necessity of a broader experimental program in order to gain more knowledge.

This paper will present the methodology and outcome of the recently conducted large scale out-of-plane experiments and companion tests that will be used as a base to construct a calculation guideline for ductile adhesive and Carbon Fiber Reinforced Plastic (CFRP) reinforced masonry.

METHODOLOGY

Building the specimens

All specimens consisted of half brick clay masonry, with material properties as presented in Table 1. The masonry wallets were produced in a total of 12 series, with 3 series being produced daily. Fresh mortar was prepared for each production batch, which was enough to build the specimens given in Table 2. Due to the relatively high suction capacity of the used clay bricks (Haller number > 4.0 kg/m2·min), the bricks were wetted using a water hose in order to prevent drying out of the mortar used. Wet cloths were placed around the masonry specimens in order to create a humid environment. An important remark is that the masonry wallettes for the bending tests, were built against a frame. This resulted in the side facing the mason having better filled mortar joints than the side facing the frame. Approximately 40% of the tested specimens had poor to bad filled mortar joints on the frame side.

A total of 174 masonry specimens with the above mentioned dimensions and 36 mortar prisms were produced. All specimens of FPBT (four point bending test) category were purposed to be reinforced. The categories CT (compression test), BWT (bond wrench test) and FT (flexural tests) were purposed for companion testing.

Table 1: Material properties of the bricks as obtained from the manufacturer Caprice.

Material property	Unit	Value
Compressive strength	MPa	≥ 10 N/mm^2
Length	mm	211 mm (±4mm)
Width	mm	101 mm (±3mm)
Height	mm	52 mm (±2mm)
Volumetric mass	kg/m^3	1660

Table 2: Prepared specimens/wallettes during each sub series

n_{series}	n_{total}	Height (mm)	Length (mm)	Width (mm)	Purpose (category)	Category
5	60	1250 (±15)	650 (±5)	101 (±3)	4 point bending tests	FPBT
2	24	350 (±10)	211 (±4)	101 (±3)	Compression tests	CT
4	48	110 (±3)	211 (±4)	101 (±3)	Bond-wrench tests	BWT
3	36	40 (±0.5)	160	40 (±0.7)	Flexural tests	FT

Reinforcing the specimens

After the specimens cured for 5-7 days, the walls were placed in a lying position (surface with less filled mortar joints facing up) on Polyethylene foam boards with a thickness of 20 mm. Afterwards the milling process took place in the following week, at which all the specimens were provided with two grooves of 15 mm in width, 65 mm in depth, and a center to center distance of 325 mm. After the milled specimens were made dust-free and were provided with a primer layer to insure higher adhesion, they were filled with the visco-elastic epoxy before pushing the CFRP strips (20 x 1.4 mm) in place at a 3 mm distance to the bottom of the groove. In order to measure the slip of the CFRP strips, the strips stuck out 25 mm from both sides of the wallets.

For the FPBT specimens, the cement based reinforcement layer with imbedded CFRP net (QSC, n=24) and polymer based reinforcement layer (QSP, n=12) were installed after the CFRP strips were placed. The reinforcement layer did not cover the bottom and top three brick layers, in order to avoid clamping and the therewith resulting disturbing effects on the experiments. Only one surface of the specimens was treated. The remaining FPBT specimens had no extra reinforcement layer (QSS, n=24). Finally, from both the top brick layer and the bottom brick layer, two steel anchors with an inter distance of 530 mm were installed on both sides at a depth of 300 mm for all the specimens. The purpose of the rods was to prevent shear failure near the support.

The material properties of the reinforcement and anchors used are provided in Table 3. A schematic view of the added reinforcement is provided in Figure 1. An overview of the different reinforced specimens is provided in Table 4 and Figure 2. The plus sign after the specimen code indicates that the treated surface will be subjected to tension due to bending, whereas the minus sign indicates the same for the non-treated surface. The amount of successfully tested specimens is lower than the amount of built specimens due to errors during transport.

Table 3: Material properties of the reinforcement used

Parameter	Unit	CFRP strip	Steel anchor	CFRP net	Cement layer	Polymer layer
Density	kg/m^3	-	7800	1790	2090	1087
Young's modulus	GPa	≥205	200	160	26	1,2
Tensile strength	MPa	≥2800	500	4300	6.5	45
Comp. strength	MPa	-	-	-	45.5	38
Max. elongation	‰ strain	>1.35	10	1.75	-	600
Thickness	mm	1.4	12	0.044	±15	±5
Grid size	mm	-	-	20 x 20	-	-
Width	mm	20	-	3	-	-

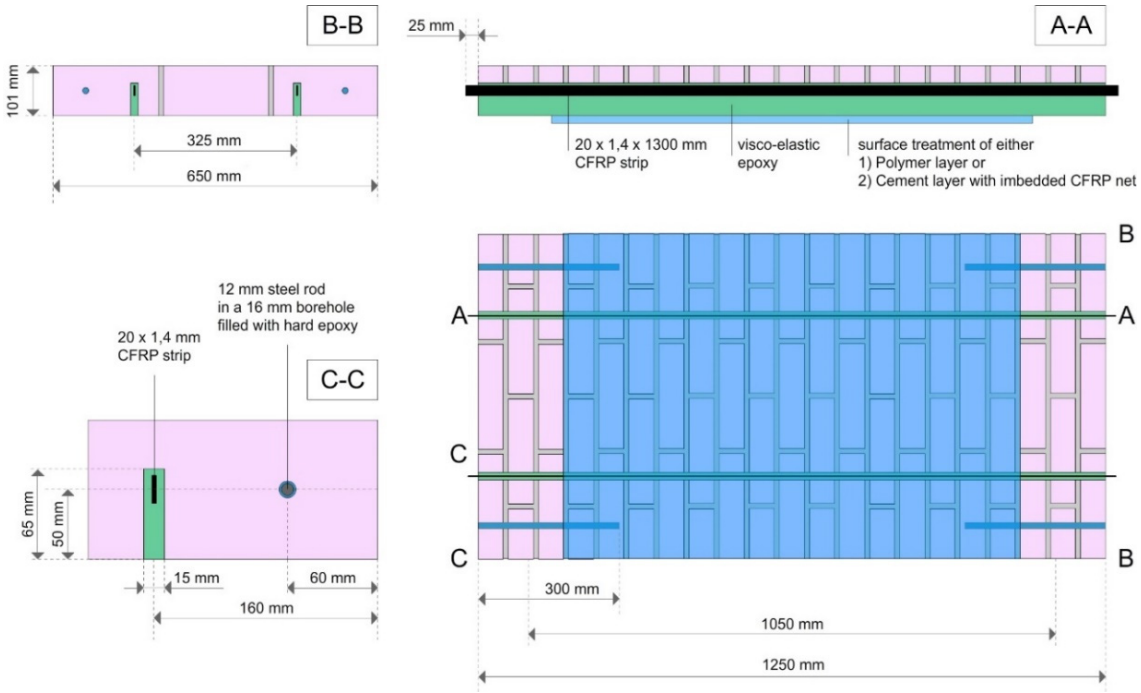

Figure 1: Schematic overview of the reinforced specimens.

Table 4: Material properties of the reinforcement used

Parameter	QSS-	QSS+	QSC-	QSC+	QSP+
n_{made}	12	12	12	12	12
n_{tested}	11	10	11	10	11
Surface reinforcement	None	None	Cement + CFRP net	Cement + CFRP net	Polymer
Tensile stresses introduced in	Non-treated side	Treated side	Non-treated side	Treated side	Treated side

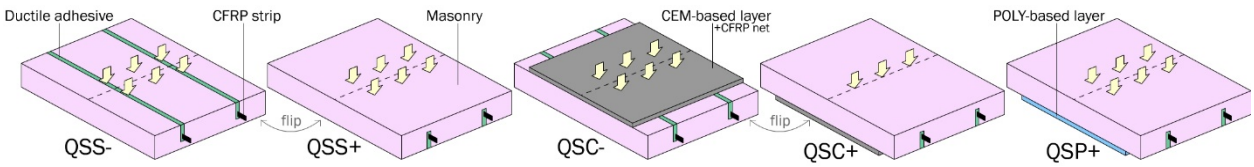

Figure 2: Overview of the different reinforced specimens.

A schematic view of the test-setup on which the four-point bending experiments were conducted is presented in Figure 3. The force is monotonic statically applied by means of a hydraulic jack, and measured with a load cell. The hydraulic jack was displacement controlled, at an average speed of 0.4 mm/s. The distribution of the applied force over the specimen is achieved by using two steel beams (length 300 mm, center to center distance 240 mm) with three rubber blocks each. The center to center distance between the two supports was 1100 mm. Five laser sensors were installed to measure the out of plane displacement of the masonry brick wallets during testing, and two laser sensors were placed to analyze the displacement above the two supports. Additionally, four LVDT sensors were installed to measure the slip of the Near Surface Mounted (NSM) CFRP strips. Figure 4 is a photo of the test installation. Figure 5 shows a detailed view of one of the four LVDT sensors, resting on the imbedded CFRP strip.

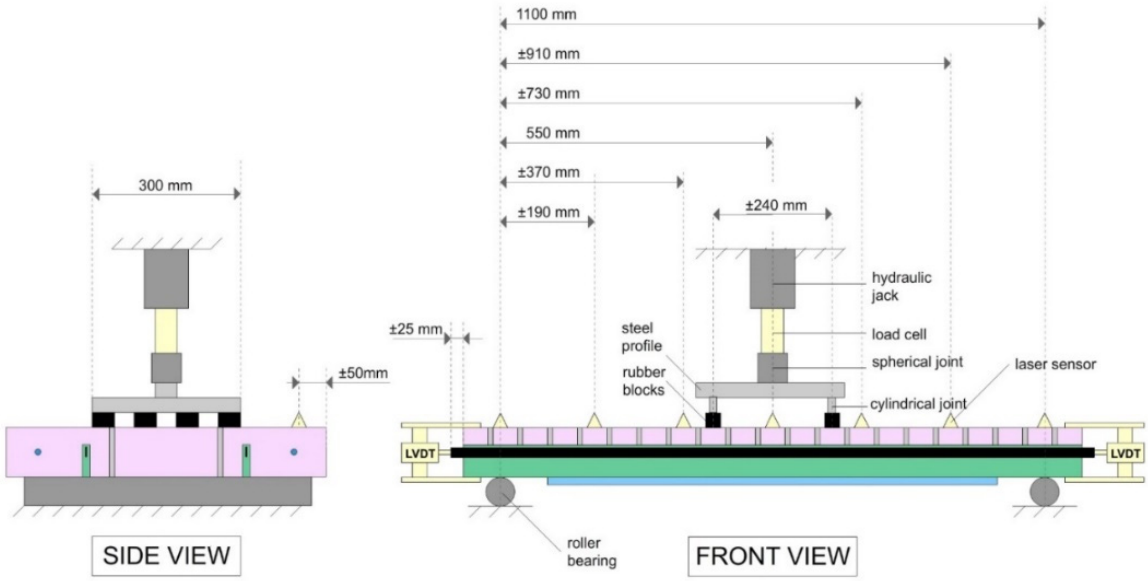

Figure 3: Schematic overview of the four-point bending test setup

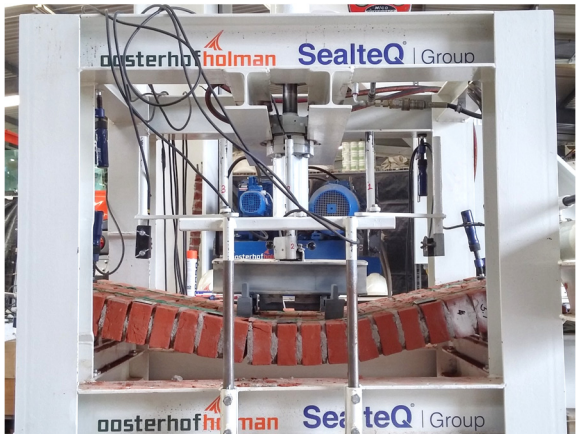

Figure 4: For point bending test set up

Figure 5: Detailed view of the LVDT

As for the material properties, the average strain and strength of the (compression) tested URM1-specimens were found to be 0.005 mm/mm (SD=0.001) and 7.079 MPa (SD = 0.718) respectively. The average flexural and compression strength of the tested mortar prisms were found to be 2.511 MPa (SD=0.272) and 6.415 MPa (SD = 0.815) respectively. The average bond strength was found to be 0.15 MPa (SD=0.057).

RESULTS

The following list presents the steps that were carried out in order to prepare the data of the conducted 4-point bending experiments for presentation:

- The laser sensors had a range of ±65mm. Figure 6 presents and illustrative overview of the measured deflections. Sensor 4 was frequently out of range due to the high deflections. When this occurred, linear extrapolation is used between (t-1) and (t-50) to construct the deflection at time t. This was especially the case after post-peak behavior was initiated.
- The maximum moment is presented as

$$M_{\max} = \left(\frac{1.10 - 0.24}{2}\right)\frac{F}{2} \tag{1}$$

- The curvature of the specimens was determined by using the least squares method. A second degree polynomial $f_i(x)$ is computed for the displacement at a given location *i*. The polynomial is constructed using the displacements at point *i-1*, *i* and *i+1*:

$$\left[x_{i-1}\ x_i\ x_{i+1}\right] \rightarrow \textit{Least squares estimate} \rightarrow \alpha_i x^2 + \beta_i x + \chi_i = d_i(x) \tag{2}$$

  After the function is obtained the second derivate, which is the curvature, is calculated with

$$\kappa_i(x) = \frac{d^2 d_i(x)}{dx^2} = 2\alpha_i \tag{3}$$

- The moment-curvature correlation will be determined for points i = 3, 4 and 5. Only the moment- curvature relation at the mid span (i=4) will be presented in the following figures.
- In order to determine the natural frequency and behavior factor for calculation purposes regarding the response spectrum, the force, displacement, moment and curvature values at 40%, 60%, 80%, 100% and 90% (post-peak) of the maximum load are provided.

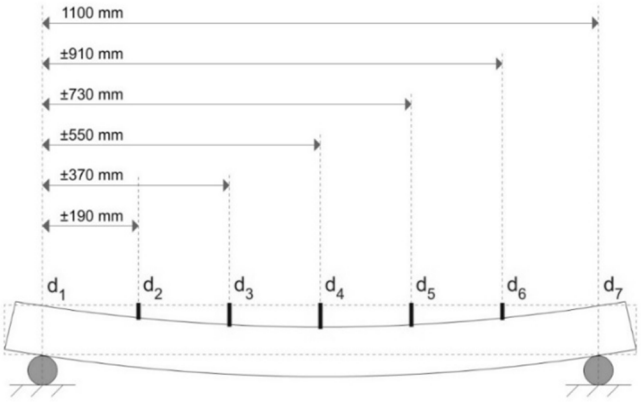

Figure 6: Illustrative overview of the measured deflections.

Figure 5 shows the load -displacement diagrams of the QSS- (A), QSS+ (B), QSP+ (C) & QSC-(D) specimens with markers at 60%, 80%, 100% and 90% (post-peak) of the force. Figure 6 shows the moment-curvature diagrams of the QSS- (A), QSS+ (B), QSP+ (C) & QSC-(D) specimens with markers at 40%, 60%, 80%, 100% and 90% (PP) of the force. The interpretation of the results will be presented in the discussion.

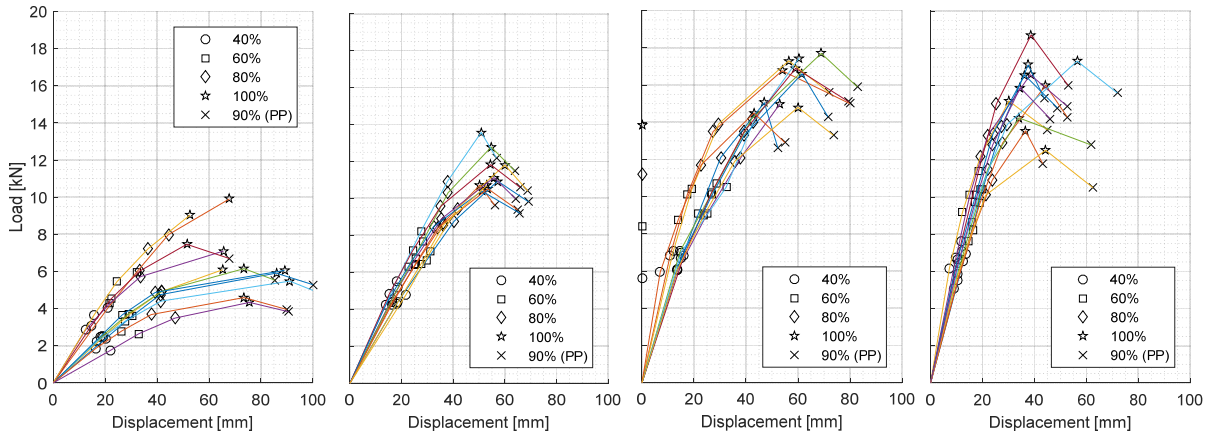

(A) **(B)** **(C)** **(D)**

Figure 5: Load -displacement diagram of all the QSS- (A), QSS+ (B), QSP+ (C) & QSC-(D) specimens with markers at 40%, 60%, 80%, 100% and 90% (PP) of the maximum force

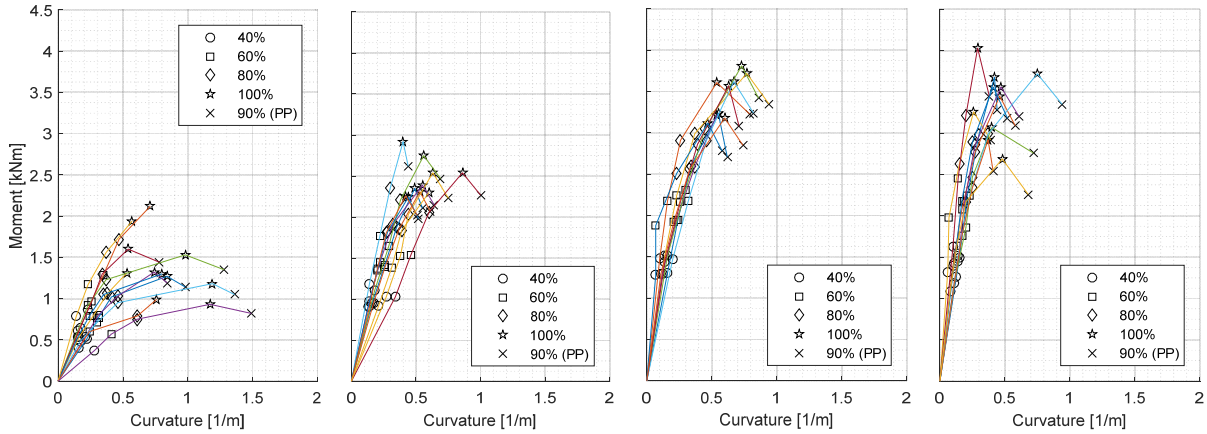

(A) **(B)** **(C)** **(D)**

Figure 6: Moment-curvature diagrams of all the QSS- (A), QSS+ (B), QSP+ (C) & QSC-(D) specimens with markers at 40%, 60%, 80%, 100% and 90% (PP) of the maximum moment

As stated earlier, rods were installed in order to prevent shear failure near the supporting points. This proved to be insufficient for the first and second specimens of QSC+ that was tested. At a force of 13.4 and 14.7 kN respectively, the out of plane experiment of the first and second failed QSC+ specimen were unsuccessful because the shear forces became critical in the region between

the tip of the imbedded rods and the joint where the cement based surface treatment was cut off. Additional steel profiles were added to these critical regions to prevent shear failure. Even though the maximum force could be increased to 20.5 kN, the shear forces remained critical.

In order to be able to gather data from the QSC+ specimens without shear becoming critical, the test set-up up was adjusted to a three-point bending configuration with a decreased center to center distance of the roller supports (from 1100 to 800mm). This resulted in the cement based surface strengthening being clamped between the specimen and the supports. With the adjusted test set-up, shear was no longer critical. The results of the remaining QSC+ specimens on this set up are presented in Figure 7.

An important remark is that the values in Figure 7 are based on the second load peak that occurred during testing of the QSC+ specimens. Figure 8 shows the load-displacement (mid-span) diagram of the QSC+8 specimen. The first peak occurs at the moment right before the imbedded CFRP net of the cement based strengthening layers fails. The CFRP strips prevent the specimen from failing, and make it possible to increase the load further. The second peak occurs when the shear stress between the CFRP strip and the QSE becomes critical.

The reason for preferring the 2nd peak despite the lower maximum load, is because of the obtained higher energy dissipation. The area under the curve before the first load peak only equals 178 Nm, whereas the area before the second load peak is significantly higher: 520 Nm.

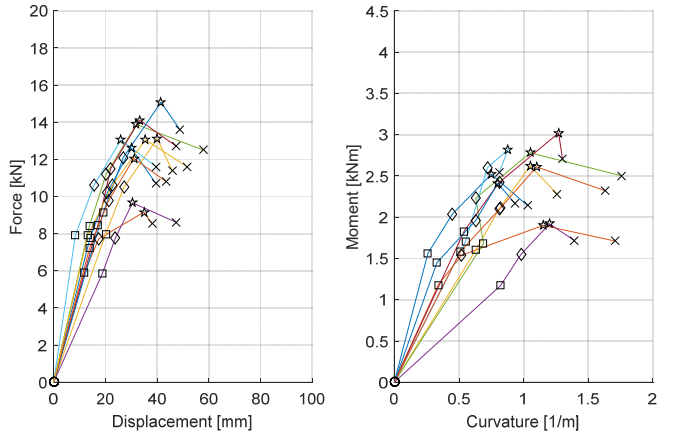

Figure 7 - Load –displacement (left) and moment-curvature (right) diagrams of all the QSC- specimens with markers as 60%, 80%, 100% and 90% (post-peak) of the force

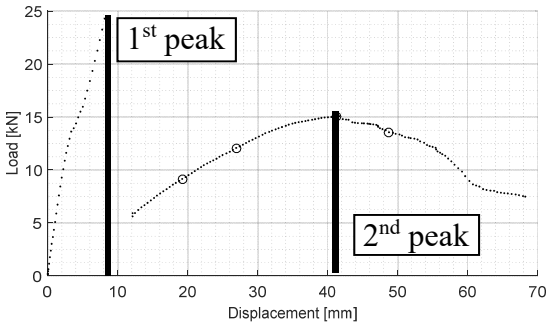

Figure 8 - Load –displacement (mid span) diagram of the QSC-8 specimen

By using the formulas obtained from the EuroCode [3], the design moment capacity for each of the reinforcement systems can be determined. These values, together with the needed parameters for calculation, are represented in Table 5.

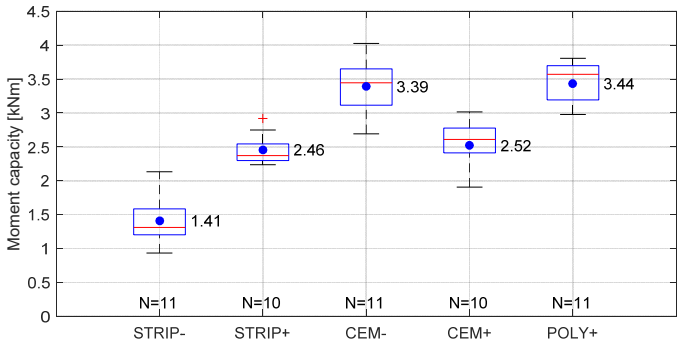

Figure 9: Box-plots of the maximum moment capacity of all tested wallettes.

Mean value $$m_x = \frac{1}{n}\sum x_i \quad (4)$$

Estimated value of the standard deviation σ for X $$s_x = \sqrt{\frac{1}{n-1}\sum (x_i - m_x)^2} \quad (5)$$

Coefficient of variation of X $$V_x = s_x / m_x \quad (6)$$

Partial factor for resistance [1] $$\gamma_m = 1,5$$

Design value of the possible conversion factor [1] $$\gamma_M = 1,0$$

The design value of the moment capacity (kNm) $$X_d = \frac{m_x}{\gamma_m \gamma_M}\{1 - k_n V_x\} \quad (7)$$

Table 5: Design moment capacity [kNm] of the reinforcement systems.

Specimen	QSS-	QSS+	QSC-	QSC+	QSP+
n	11	10	11	10	11
m_x	1.410	2.459	3.395	2.522	3.438
s_x^2	0.137	0.051	0.149	0.130	0.086
V_x	0.262 *(0.090)*	0.092	0.114	0.143	0.085
k_n*	1.92	1.92	1.92	1.92	1.92
X_d	**0.467** *(0.764)*	**1.349**	**2.769**	**1.214**	**1.916**

* 5% characteristic fractile factor

DISCUSSION

From the measurement of the slip of the CFRP strips for the QSS+ specimens it can be concluded that the resistance of the specimens is determined by the bond capacity of the CFRP strips. When the maximum load is reached, the free-end slip of the CFRP strips increases significantly. A typical behavior of the slip is shown in Figure 10. When the maximum force is reached, the slip in both strips (1 & 2) increases significantly on the free-end side of one of the wall sub-panels (in this case sub-panel A). The resulting wall sub-panels are subsequent to a fully developed crack pattern, where the specimen starts to behave as two rigid bodies that rotate around the main crack line. The free-end side of sub-panel B shows a decrease in slip with decreasing force.

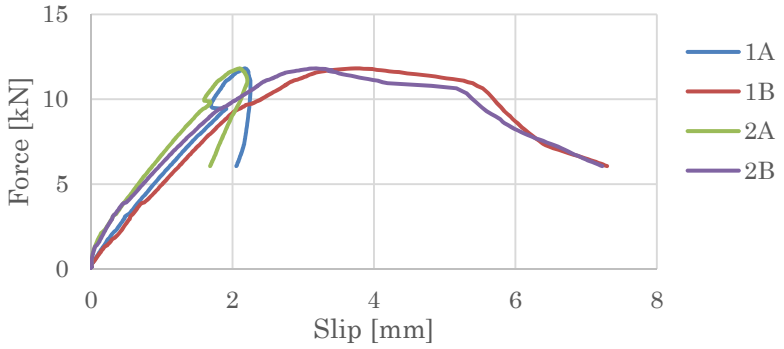

Figure 10: Slip of CFRP strips of specimen QSS+3. 1A and 1B represent the slip of the strip #1 at the left (A) & right side (B) respectively. Same applies for 2A & 2B for strip #2.

The resistance of the QSS- specimens was lower than that of the QSS+ specimens due to the relatively badly filled mortar joints on the reinforced side of the masonry wallettes. The coefficient of variation of the QSS- specimens was found on the high side (0.262 kNm) when compared to the coefficient of variation of the QSS+, QSC- and QSP+ specimens (0.092, 0.114 and 0.085 respectively). This resulted in the design moment capacity of QSS- being very low: 41% of the mean value. If a reduced coefficient for the variation of 0.090 is applied, which is more in range with the QSS+ specimen, the design value for the moment capacity will become 1.042 kNm. Also for this configuration the slip of the CFRP strips was increasing on one side of the strip from the moment the maximum capacity was reached.

The resistance of the QSP+ specimens was found to be greater than that of the QSS+ specimens. The polymer reinforcement layer is compatible with the imbedded CFRP strips due to its high deformation capacity, resulting in an increase of 35% in the design moment capacity of the QSP+ specimens compared to the case with no additional polymer layer (QSS+).

The behavior of the QSC+ specimens is quite different from the behavior of the other configurations. The cement reinforcement layer is not compatible with the imbedded CFRP strips due to stiff behavior, resulting in a two-stage failure mechanism. With the added cement layer there is a significant increase in initial stiffness and capacity. After the imbedded CFRP net of the cement based strengthening layers fail in tension, the imbedded CFRP strips are activated and the resistance of the specimen drops back and the specimen start to behave similar to the QSS+ specimens. This sudden activation process does not lead to a degradation in ultimate moment capacity compared to the case with a single-stage failure mechanism (QSS+).

The resistance of the QSC- specimens was found to be higher than the QSS+ specimens. Adding 15 mm of reinforcing cement layer on a specimen initially reinforced with centrally placed CFRP strips, leads to an increase of 40% in the moment capacity compared to the case with no additional cement layer. This is likely caused by the more beneficial internal moment arm and increased capacity of the compression zone.

CONCLUSIONS

The conducted four-point bending and three-point bending experiments for the various configurations resulted in design values for the moment capacity of 0.764 kNm (QSS-, n=11), 1.349 kNm (QSS+, n=10), 2.769 kNm (QSP+, n=11), 1.214 kNm (QSC+, n=10) and 1.916 kNm (QSC-, n=11). From the measurement of the slip of the imbedded CFRP strips it can be concluded that the resistance of the specimens is primarily determined by the bond capacity of the CFRP strips. The polymer reinforcement layer is compatible with the imbedded CFRP strips due to its high deformation capacity. This is not the case for the cement reinforcement layer due to stiff behavior. This results in a two-stage failure mechanism where the imbedded CFRP strips are activated after the cement based strengthening layers fail in tension.

The observed deformation capacities and maximum withstandable loads show that CFRP reinforcement with visco-elastic adhesive remains a promising solutions to improve the seismic performance of buildings in Groningen.

RECOMMENDATIONS

The following recommendations are made for improving the current method of testing:

- Increase the measuring range of the mid-span deflection laser sensors and of the LVDT's.
- Improve the steel profile that transfers the force from the hydraulic jack to the specimen, so that the force can be distributed more evenly over the width of the specimen.
- Measure the deflection at three different locations with the same moment, so a more precise estimation of the moment-curvature correlation can be constructed.

The following recommendations are made in order to get more insight on the bond slip behavior:

- Perform direct and beam pull-tests to gain more knowledge on the bond-slip behavior of CFRP strips imbedded in the visco-elastic epoxy.

Finally, another aspect that should be taken into account is the introduction of cyclic loading to investigate degradation effects. This is especially important for cyclic earthquake loads.

ACKNOWLEDGEMENTS

The authors wish to thank and acknowledge QuakeShield, Royal Oosterhof Holman and SealteQ for supporting this research into the behavior of a new seismic retrofit systems.

REFERENCES

[1] NPR 9998 (2015). "Assessment of structural safety etc., seismic loads induced earthquakes" (In Dutch: "Beoordeling van de constructieve veiligheid van een gebouw bij nieuwbouw, verbouw en afkeuren - Grondslagen voor aardbevingsbelastingen: Geïnduceerde aard-bevingen"), *NEN*, Delft, Netherlands.

[2] Türkmen, Ö.S., Vermeltfoort, A.T. and Martens, D.R.W. (2016). "Seismic retrofit system for single leaf masonry buildings in Groningen." *Proc., 16th International Brick and Block Masonry Conference*, Padova, Italy, on USB.

[3] EN 1990: Eurocode: Basis of Structural Design: BSI April 2002.